Electronic Supplementary Information (ESI)

Green self-activation engineering of metal-organic frameworks derived hollow nitrogen-doped carbon spheres towards supercapacitors

Jinyang Zhang, Dongxu Wu, Qian Zhang, Anning Zhang, Jinfeng Sun, Linrui Hou*, Changzhou Yuan*

School of Materials Science and Engineering, University of Jinan, Jinan 250022, P. R. China

E-mail: mse_houlr@ujn.edu.cn (*Prof.* Hou)

mse_yuancz@ujn.edu.cn; ayuancz@163.com (*Prof.* Yuan)

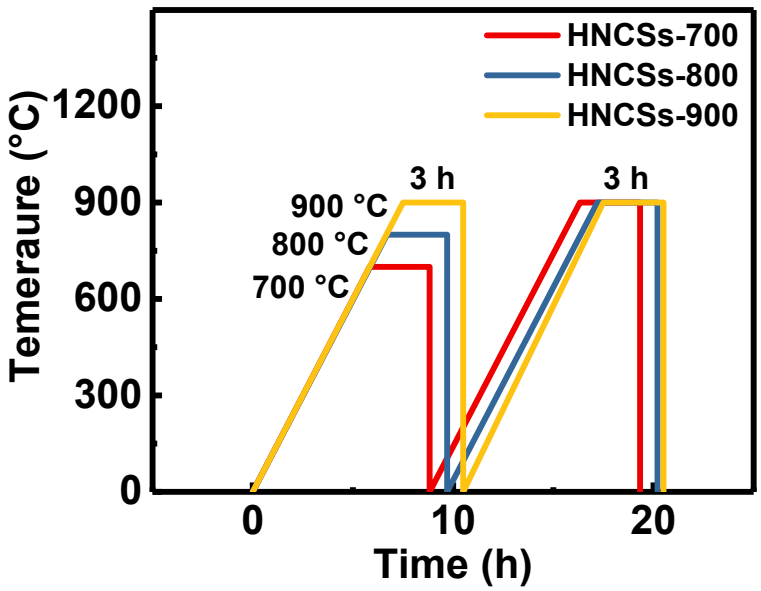

Fig. S1 Schematic illustration for the two-step calcination process towards synthesis of HNCSs-700, HNCSs-800, and HNCSs-900.

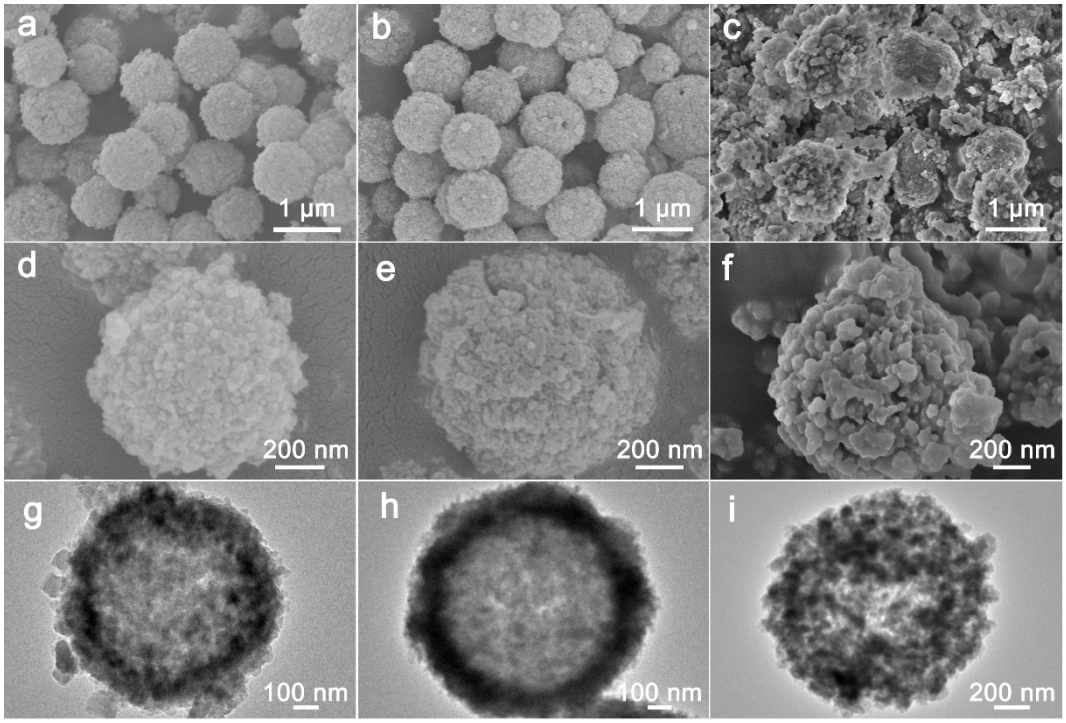

Fig. S2 (a – f) FESEM and (g – i) TEM images of (a, d, g) HZMSs-2, (b, e, h) HZMSs-4 and (c, f, i) HZMSs-8.

The FESEM images of HZMSs-x (x=2, 4, 8) (**Fig. S2**) all also display the hollow microspheres (HMSs). The average diameters of HZMSs-2, HZMSs-4 and HZMSs-8 (**Fig. S2**a-f) are ~860, ~1000 and ~1190 nm, respectively, which gradually augment with the increasing temperature. On the contrary, the average shell sizes of HZMSs-2, HZMSs-4 and HZMSs-8 (**Fig. S2**g-i) are ~170, ~180 and ~460 nm, suggesting that the higher solvothermal temperature applied can accelerate cavitation process.

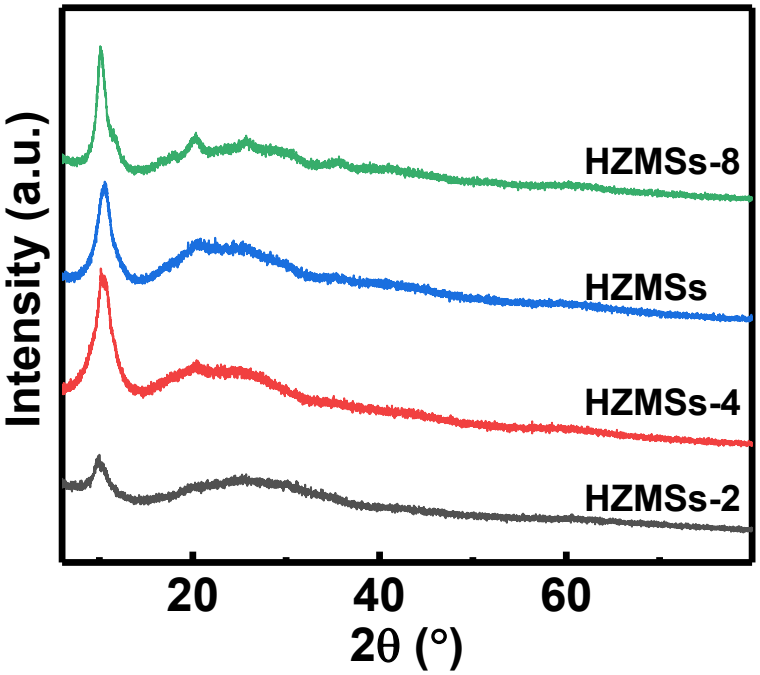

Fig. S3 XRD patterns of HZMSs, HZMSs-2, HZMSs-4 and HZMSs-8.

The full width at half maximum of the diffraction peak at 10.7° decreases from 1.4° to 1.1°, and the diffraction peaks located at 2θ range from 10.7 to 21.2° become more obvious, suggesting that the crystallization degree of the samples increases with the increasing solvothermal temperature.

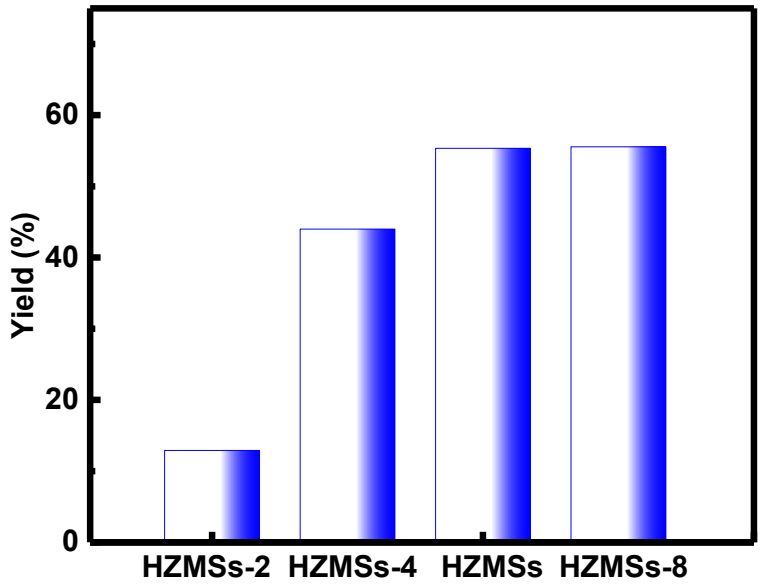

Fig. S4 Yields of the HZMSs and HZMSs-x (x = 2, 4, 8).

The yields of HZMSs and HZMSs-x (x=2, 4, 8) are calculated based on the content of $Zn(NO_3)_2 \cdot 6H_2O$, corresponding to 55.3%, 12.9%, 44.0%, and 55.3%, respectively (**Fig. S4**). This result indicates that the reaction progress is basically stable when the solvothermal temperature increases to 160 °C.

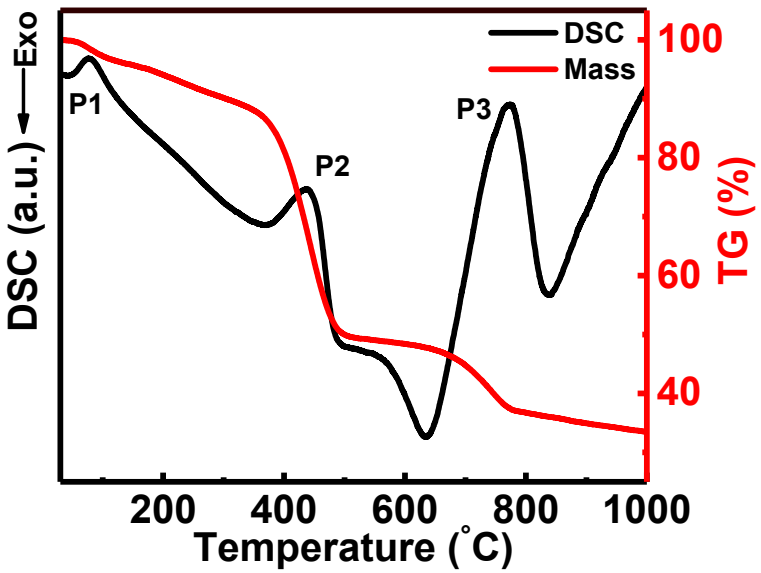

Fig. S5 DSC and TG curves of HZMSs.

DSC curve displays three broad endothermic peaks corresponding to the loss of adsorbed water (P1, 79 °C), the pyrolysis process (P2, 438 °C) and volatilization of Zn (P3, 773 °C), which accords with the obvious mass losses on the TG curve.

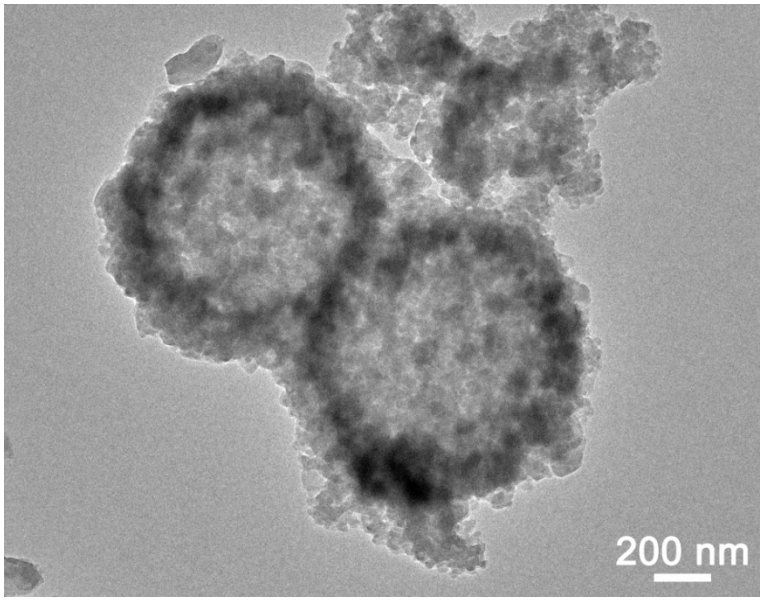

Fig. S6 TEM image of the product obtained just after solvothermal treatment for 0.5 h at 160 °C.

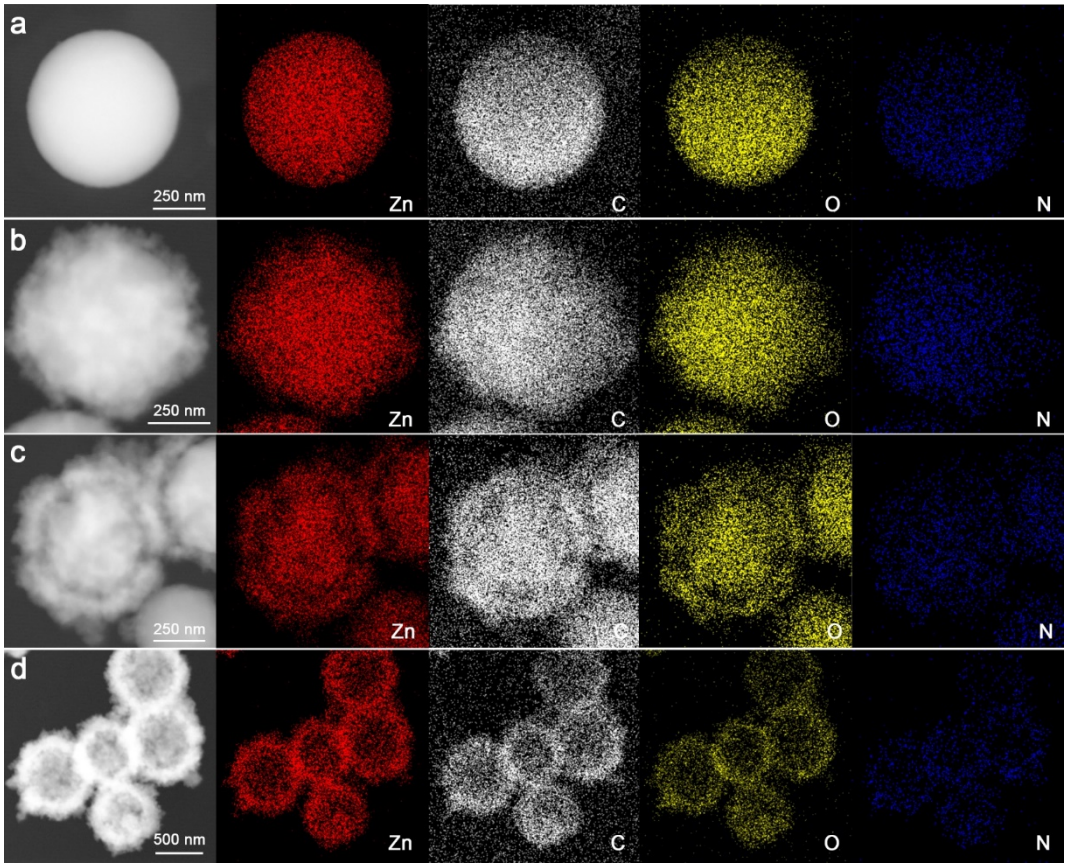

Fig. S7 STEM images and corresponding element mapping images of Zn, C, O and N for (a) SZMSs, (b) CSZMSs, (e) YSZMSs and (f) HZMSs-1.

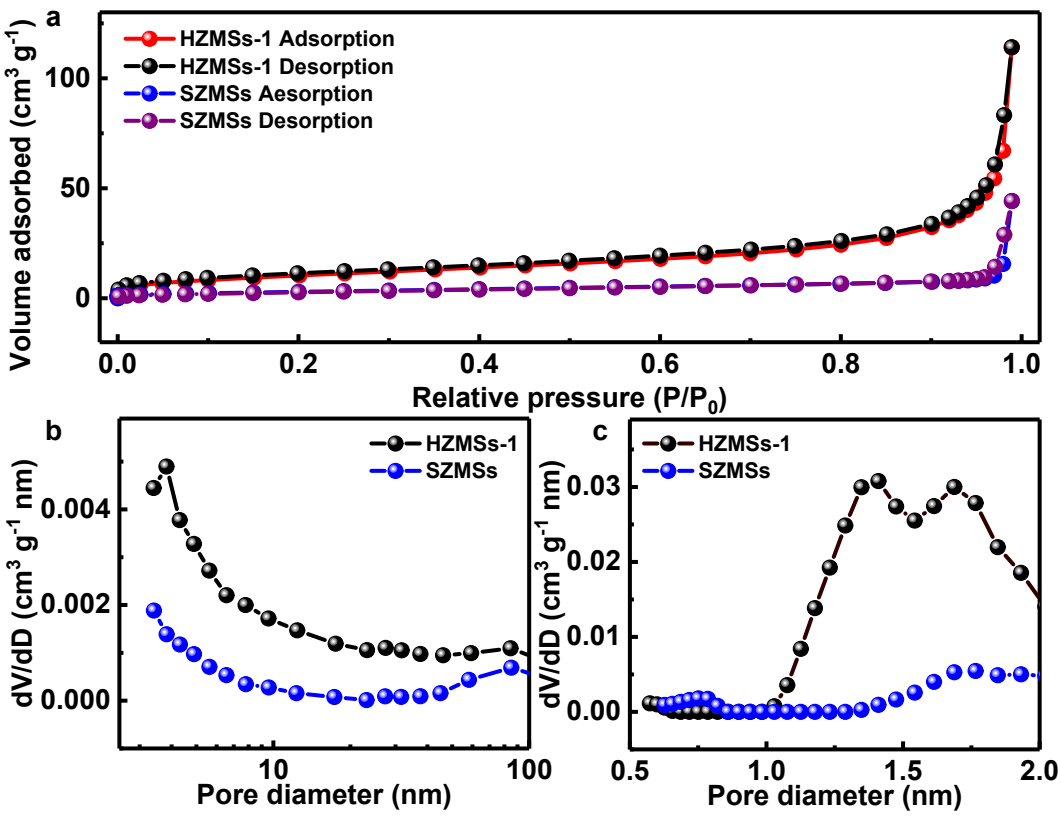

Fig. S8 (a) N_2 ad-/desorption isotherms, (b) mesopore/macropore and (c) micropore size distribution plots for the SZMSs and HZMSs-1.

The N_2 ad-/desorption isotherms of SZMSs and HZMSs-1 (**Fig. S8**a) are used to quantify the pore structure, which belong type IV isotherms with a H3-type hysteresis loop. Besides, the N_2 ad-/desorption capacity of HZMSs-1 is significantly higher than that of SZMSs. To be specific, the HZMSs-1 has a higher specific surface area (~38.4 m^2 g^{-1}) and a larger total pore volume (~0.18 cm^3 g^{-1}) than that of SZMSs (~11.0 m^2 g^{-1}, ~0.07 cm^3 g^{-1}). According the pore size distribution plots (**Fig. S8**b, c), the average pore size of HZMSs-1 is ~18.4 nm, smaller that of the SZMSs (~24.9 nm). Therefore, it is easy to conclude that the solvothermal time plays an important role in promoting the formation of HZMSs-1 with more abundant pores.

Table S1 The atomic percent of Zn, C, O, N in the SZMSs, CSZMSs, YSZMSs and HZMSs-1

Sample	Zn	C	O	N	C/Zn
SZMSs	5.2	76.7	17.0	1.1	14.75
CSZMSs	5.1	75.1	18.6	1.2	14.72
YSZMSs	4.9	74.8	19.3	1.0	15.27
HZMSs-1	4.5	74.3	20.1	1.1	16.51

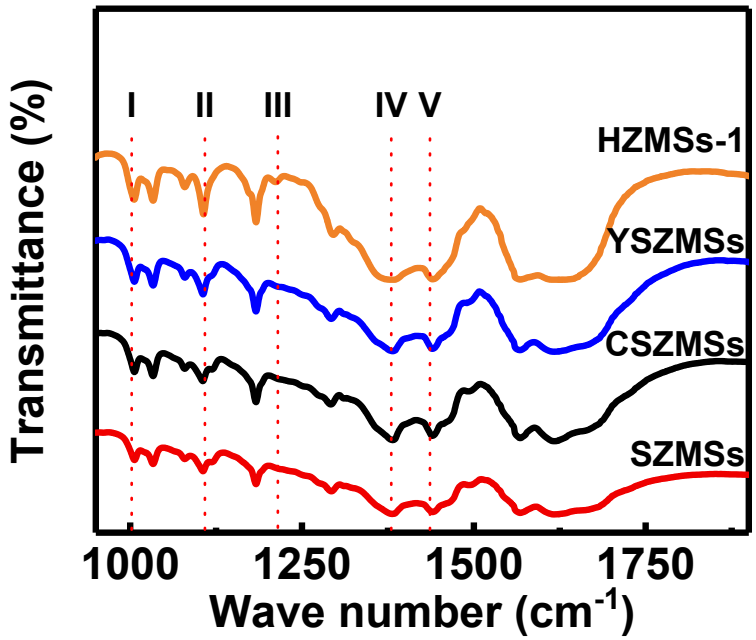

Fig. S9 FT-IR spectra of the SZMSs, CSZMSs, YSZMSs and HZMSs-1.

The functional groups of organic-ligand are discerned by analyzing the FT-IR spectra (**Fig. S9**). The bands at 1015 cm^{-1} (I) and 1095 cm^{-1} (II) are assigned to the para-aromatic C-H.[1-3] Besides, the band (III) at 1217 cm^{-1} represent the stretching vibrations of the NO_2 group,[4] which disappears in HZMSs-1. In addition, the band (IV) at 1370 cm^{-1} is ascribed to stretching vibration of $-COO^-$.[5] Furthermore, the band (V) at 1415 cm^{-1} is attributed to the stretching vibrations of C-N from DMF.[1,6]

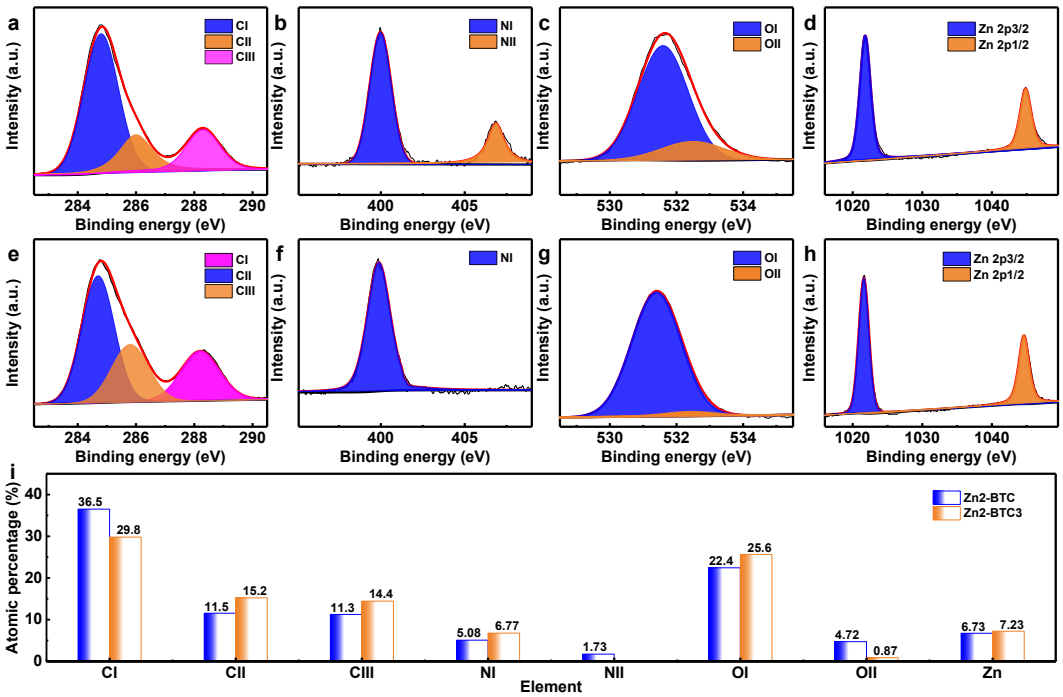

Fig. S10 High resolution elemental XPS spectra of (a – d) SZMSs and (e – h) HZMSs-1, and (i) atomic percentage of different function group.

In order to further confirm the elemental composition and chemical bond of SZMSs and HZMSs-1 samples, the XPS was conducted, and detailed results are collected in **Fig. S10**. The C 1s (**Fig. S10**a, e) can be subdivided into three peaks at ~284.8 (CI), ~286.0 (CII) and ~288.3 eV (CIII), which are ascribed to the C–C/C=C, C–O/C–N and O-C=O groups.[7] the N 1s spectra (**Fig. S10**b, f) show three peaks at ~400.0 (NI) and ~406.9 eV (NII), which are attributed to the C-N and N-O groups, respectively.[8] Meanwhile, the high-resolution O 1s spectra (**Fig. S10**c, g) mainly present two oxygen species, that is, O=C/Zn-O (OI, ~531.6 eV)[9,10] and O-N/C-OH (OII, ~532.5 eV)[11]. As for the Zn 2p spectra (**Fig. S10**d, h), the peaks centered at ~1021.8 and ~1044.9 eV, confirming the presence of Zn-O.[9] Therefore, the disappearance of N-O functional group suggests that the phase structure has changed between HZMSs-1 and SZMSs.

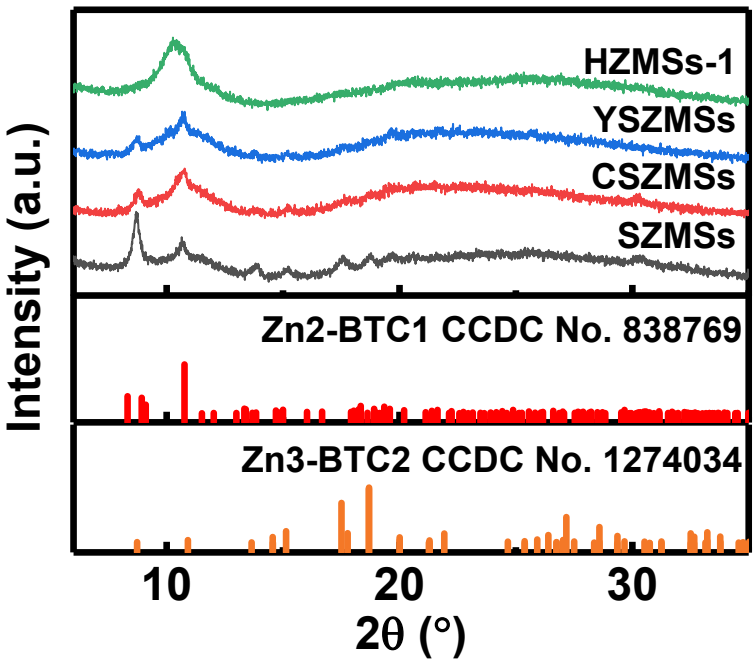

Fig. S11 XRD patterns of SZMSs, CSZMSs, YSZMSs and HZMSs-1.

Some obvious diffraction peaks appear at 8.7, 10.7, 13.8 and 17.6 ° for SZMSs. However, just one obvious peak appears at 10.7 ° in HZMSs-1. It demonstrates that the Zn2-BTC1 (CCDC No. 838769) structure for SZMSs has transformed into Zn3-BTC2 (CCDC No. 1274034) structure in HZMSs-1.[12,13]

Table S2 Summary of SSA_{total}, SSA_{mic}, SSA_{meso}, APS and V_{total} data for some reported carbon nanomaterials

Sample	SSA_{total} ($m^2\ g^{-1}$)	SSA_{mic} ($cm^2\ g^{-1}$)	SSA_{meso} ($cm^2\ g^{-1}$)	APS (nm)	V_{total} ($cm^3\ g^{-1}$)	Refs.
CNT-HCS	500.8	~	~	~	0.55	14
HCS-2	670.0	~	~	~	0.44	15
C/KOH-700	1113	889	224	1.1-2.4	0.68	16
N-HMCSs	750	~	~	~	1.01	17
MnO_2/HCS-30	379	299	71	3.9	0.21	18
N-HCS	911	581	~	~	0.92	19
SO-HCS	670	~	~	~	0.91	20
NHCS-E10	306	131	~	~	0.23	21
IPHHCSs	951	~	~	~	0.86	22
NHCSs	112.4	~	~	1.21	0.34	23
N-HMCS-0.1	876	~	~	~	1.6	24

Table S3 Summary of XPS data for the HNCSs-700, HNCSs-800, and HNCSs-900 samples

HNCSs-700	Binding energy (eV)	Ratio (at.%)	HNCSs-800	Ratio (at.%)	HNCSs-900	Ratio (at.%)
C 1s		89.1		91.7		92.2
C-I	284.8	50.7	C-I	61.7	C-I	46.8
C-II	286.2	21.2	C-II	20.9	C-II	16.8
C-III	289.0	17.1	C-III	9.1	C-III	28.6
N 1s		4.5		4.4		3.9
N-6	398.6	2.6	N-6	1.2	N-6	0.6
N-5	400.1	1.0	N-5	2.7	N-5	2.2
N-Q	401.5	0.9	N-Q	0.5	N-Q	1.1
O 1s		6.4		3.9		3.9
O-I	531.6	4.9	O-I	1.0	O-I	1.4
O-II	532.5	0.7	O-II	1.2	O-II	1.9
O-III	533.6	0.7	O-III	1.7	O-III	0.6

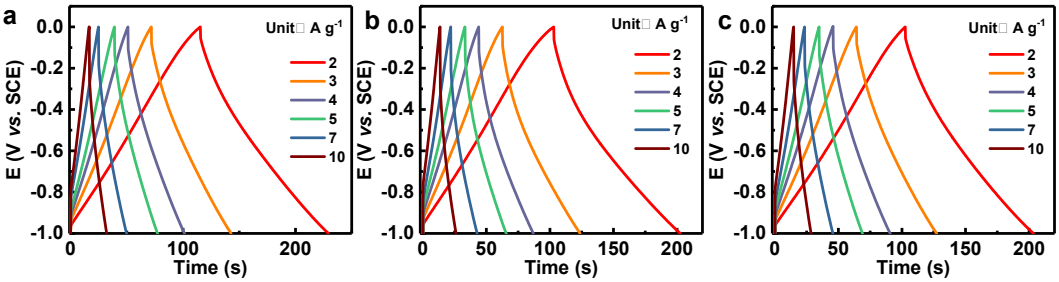

Fig. S12 GCD plots of (a) HNCSs-900, (b) HNCSs-700 and (c) HNCSs-800 at various current densities from 2 to 10 A g^{-1} in the three-electrode systems.

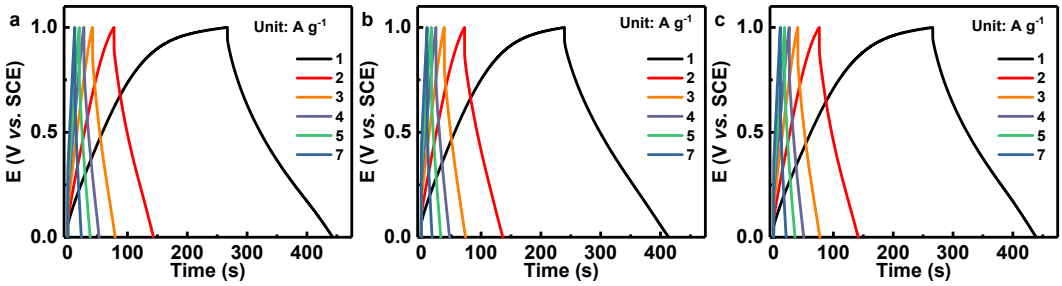

Fig. S13 GCD curves of the HNCSs-900 in the three-electrode systems for (a) 1 M Na_2SO_4, (b) 1 M Li_2SO_4 and (c) 1 M K_2SO_4 aqueous electrolyte at various current densities from 1 to 7 A g^{-1}.

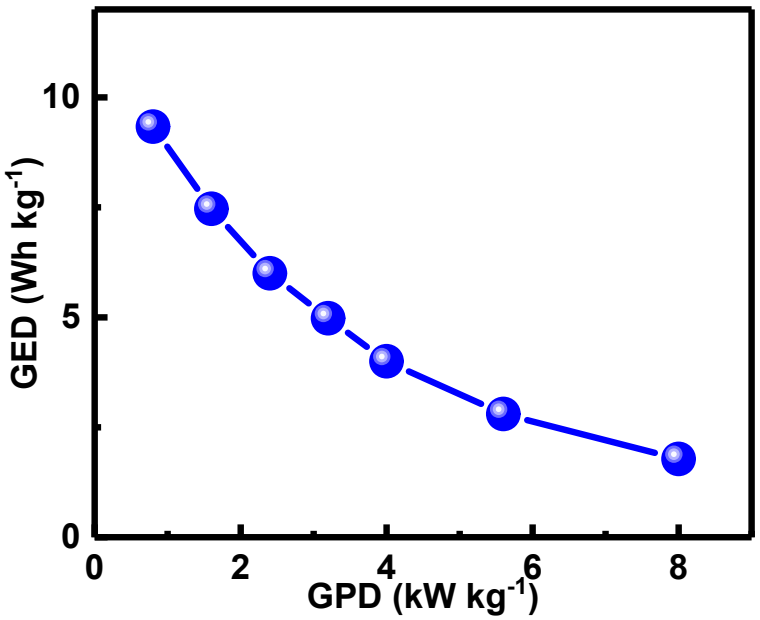

Fig. S14 Ragone plots of the assembled HNCSs-900//HNCSs-900 cell.

Table S4 Comparison of GSC between HNCSs-900 and some reported carbon nanomaterials in three-electrode system

Sample	Electrolyte	Current density ($A\ g^{-1}$)	GSC ($F\ g^{-1}$)	Active material loading ($mg\ cm^{-2}$)	Refs.
HNCSs-900	**6 M KOH**	**1**	**254.6**	**5.0**	**our work**
HNCSs-900	**1 M H_2SO_4**	**1**	**284.4**	**5.0**	**our work**
CNT-HCS	6 M KOH	0.5	201.5	~	14
HCS-2	6 M KOH	0.5	160.8	2-3	15
C/KOH-700	6 M KOH	1	295	4-5	16
HPGS	6 M KOH	1	227	3	25
N-HMCSs	6 M KOH	1	170	7-8	17
MnO_2/HCS-30	1 M Na_2SO_4	1	255	3	18
N-HCS	6 M KOH	0.5	173	7-8	19
SO-HCS	1 M H_2SO_4	0.1	210.7	~	20
NHCS-E10	6 M KOH	0.5	125	~	21
IPHHCSs	6 M KOH	1	295	2.2	22
NHCSs	6 M KOH	0.5	263.6	3-6	23
N-HMCS-0.1	6 M KOH	0.5	307	4-5	24

Table S5 Comparison of self-discharge rates for supercapacitors using aqueous electrolytes

Devices	OCVs decay rate (V)	Leakage current（mA）	Electrolyte	Refs.
HNCSs//HNCSs	**1.6-1.2 for 5 h**	**0.011**	**1 M Na_2SO_4**	**This work**
NSHPC//NSHPC	1.0-0.74 for 24 h	0.156	6 M KOH	26
TBC-K1.1//TBC-K1.1	0.9-0.26 for 24 h	0.15-0.17	1 M H_2SO_4	27
AC_{TS}-1.0//AC_{TS}-1.0	1.0-0.83 for 1 h	0.02	6 M KOH	28
$NiCo_2O_4$@NC//rGO	1.5-1.3 for 24 h	0.02	6 M KOH	29
NiO/DSM-C//DSM-C	1.4-0.5 for 24 h	0.06	6 M KOH	30
NiS/rGO//IHPC	1.6-0.75 for 24 h	1.7	6 M KOH	31
NS-132//NS-132	1.7-0.83 for 22 h	106	1 M Li_2SO_4	32
Asn-5-$NaHCO_3$//Asn-5-$NaHCO_3$	1-0.62 for 1 h	0.018	6 M KOH	33

Table S6 Comparison of electrochemical properties between HNCSs-900 and previously reported carbonaceous materials for symmetrical supercapacitor

Devices	Voltage window (V)	Electrolyte	GED (Wh kg^{-1}) /GPD (kW kg^{-1})	Reference
HNCSs-900//HNCSs-900	**0-1.6 V**	**1 M Na_2SO_4**	**9.3/0.8**	**our work**
CNT-HCS-1.2//CNT-HCS-1.2	0-1.6 V	1 M Na_2SO_4	~3/1	14
CNT-HCS//CNT-HCS	0-1.6 V	1 M Na_2SO_4	11.3/0.13	14
HCS-2//HCS-2	0-1 V	6 M KOH	6.2/0.025	15
C/KOH-700//C/KOH-700	0-1 V	6 M KOH	8.3/1.1	16
C-700//C-700	0-1 V	6 M KOH	2.7/0.9	16
HPGS//HPGS	0-1.2 V	6 M KOH	8.7/0.6	25
N-HMCS-0.1//N-HMCS-0.1	0-0.8 V	6 M KOH	11.2/0.7	24
N300-F-AC//N300-F-AC	0-1 V	6 M KOH	2.54/0.7	34
L-700//L-700	0-1 V	6 M KOH	8.5/0.1	35
CPC-5-700//CPC-5-700	0-1 V	6 M KOH	8.8/0.1	36
ACJM//ACJM	0-1.2 V	1 M H_2SO_4	9.9/0.53	37

References

1. Q. Liu, L. Xie, X. Shi, G. Du, A. M. Asiri, Y. Luo and X. Sun, *Inorg. Chem. Front.*, 2018, **5**, 1570.
2. L. Xu, E. Y. Choi and Y. U. Kwon, *Inorg. Chem. Commun.*, 2008, **11**, 1190.
3. M. Hema, S. Selvasekarapandian, D. Arunkumar, A. Sakunthala and H. Nithya, *J. Non-Cryst. Solids*, 2009, **355**, 84.
4. T. Weingand, S. Kuba, K. Hadjiivanov and H. Knözinger, *J. Catal.*, 2002, **209**, 539.
5. M. R. Johan, K. Si-Wen, N. Hawari and N. A. K. Aznan, *Int. J. Electrochem. Sci.*, 2012, **7**, 4942.
6. A. Paredes-Nunez, D. Lorito, N. Guilhaume, Y. Schuurman and F. Meunier, *Catal. Today*, 2019, **336**, 84.
7. S. J. Zhuo, Y. Y. Guan, H. Li, J. Fang, P. Zhang, J. Y. Du and C. Q. Zhu, *Analyst*, 2019, **144**, 656.
8. X. Zhang, W. H. Hu, L. Pei, S. P. Zhao, C. Y. Zhang and Z. Wang, *High Perform. Polym.*, 2020, **32**, 1.
9. N. K. Gupta, J. Bae, S. Kim and K. S. Kim, *Chemosphere*, 2021, **274**, 129789.
10. J. Y. Zhang, Z. Y. Chen, G. Y. Wang, L. R. Hou and C. Z. Yuan, *Appl. Surf. Sci.*, 2020, **533**, 147511.
11. O. Rosseler, M. Sleiman, V. N. Montesinos, A. Shavorskiy, V. Keller, N. Keller, M. I. Litter, H. Bluhm, M. Salmeron and H. Destaillats, *J. Phys. Chem. Lett.*, 2013, **4**, 536.
12. X. R. Hao, X. L. Wang, K. Z. Shao, G. S. Yang, Z. M. Su and G. Yuan,

Crystengcomm, 2012, **14**, 5596.

13. O. M. Yaghi, H. Li and T. L. Groy, *J. Am. Chem. Soc.*, 1996, **118**, 9096.
14. Q. Wang, J. Yan, Y. B. Wang, G. Q. Ning, Z. J. Fan, T. Wei, J. Cheng, M. L. Zhang and X. Y. Jing, *Carbon*, 2013, **52**, 209.
15. X. D. Yang, Y. L. Li, P. X. Zhang, L. N. Sun, X. Z. Ren and H. W. Mi, *Carbon*, 2020, **157**, 70.
16. F. Gao, J. Y. Qu, C. Geng, G. H. Shao and M. B. Wu, *J. Mater. Chem. A*, 2016, **4**, 7445.
17. A. B. Chen, Y. Q. Li, Y. F. Yu, S. F. Ren, Y. Y. Wang, K. C. Xia and S. H. Li, *J. Alloys Compd.*, 2016, **688**, 878.
18. W. Du, X. N. Wang, J. Zhan, X. Q. Sun, L. T. Kang, F. Y. Jiang, X. Y. Zhang, Q. Shao, M. Y. Dong, H. Liu, V. Murugadoss and Z. H. Guo, *Electrochim. Acta*, 2019, **296**, 907.
19. M. Liu, Y. F. Yu, B. B. Liu, L. Liu, H. J. Lv and A. B. Chen, *J. Alloys Compd.*, 2018, **768**, 42.
20. H. R. Wang, H. W. Zhou, M. Gao, Y. A. Zhu, H. T. Liu, L. Gao and M. X. Wu, *Electrochim. Acta*, 2019, **298**, 552.
21. F. Liu, R. L. Yuan, N. Zhang, C. C. Ke, S. X. Ma, R. L. Zhang and L. Liu, *Appl. Surf. Sci.*, 2018, **437**, 271.
22. J. Cheng, Y. C. Liu, X. X. Zhang, X. F. Miao, Y. Q. Chen, S. J. Chen, J. H. Lin and Y. N. Zhang, *Chem. Eng. J.*, 2021, **419**, 129649.
23. D. W. Zhang, S. D. Shen, X. Z. Xiao, D. S. Mao and B. M. Yan, *RSC Adv.*, 2020,

10, 26546.

24. J. Du, A. B. Chen, L. Liu, B. Li and Y. Zhang, *Carbon*, 2020, **160**, 265.
25. C. L. Chen, T. Liang, X. Chen, B. S. Zhang, L. Wang and J. Zhang, *Carbon*, 2018, **132**, 8.
26. D. Y. Zhang, M. Han, B. Wang, Y. B. Li, L. Y. Lei, K. J. Wang, Y. Wang, L. Zhang and H. X. Feng, *J. Power Sources*, 2017, **358**, 112.
27. S. Perez-Rodriguez, O. Pinto, M. T. Izquierdo, C. Segura, P. S. Poon, A. Celzard, J. Matos and V. Fierro, *J. Colloid Interface Sci.*, 2021, **601**, 863.
28. Z. W. Ma, H. Q. Liu and Q. F. Lü, *J. Energy Storage*, 2021, **40**, 102773.
29. J. Li, Y. Liu, D. Zhan, Y. J. Zou, F. Xu, L. X. Sun, C. L. Xiang and J. Zhang, *J. Energy Storage*, 2021, **39**, 102665.
30. Z. T. Zhu, F. Gao, Z. H. Zhang, Q. R. Zhuang, H. Yu, Y. Q. Huang, Q. Y. Liu and M. Fu, *J. Colloid Interface Sci.*, 2021, **603**, 157.
31. D. Y. Zhang, S. Y. Gao, J. W. Zhang, J. R. Wang, W. N. She, K. J. Wang, X. Xia, B. A. Yang and X. X. Meng, *J. Power Sources*, 2021, **514**, 230590.
32. H. Q. Tan, H. Huang, Z. X. Guan, Y. X. Qian, Y. F. Deng and G. H. Chen, *Electrochim. Acta*, 2020, **354**, 136639.
33. H. Zhou, Y. M. Zhou, S. M. Wu, L. Li, Y. H. Li, M. X. Guo, Z. C. Qi and C. X. Feng, *J. Alloys Compd.*, 2020, **829**, 154549.
34. N. F. He, S. Yoo, J. J. Meng, O. Yildiz, P. D. Bradford, S. Park and W. Gao, *Carbon*, 2017, **120**, 304.
35. F. Y. Liu, Z. X. Wang, H. T. Zhang, L. Jin, X. Chu, B. N. Gu, H. C. Huang and

W. Q. Yang, *Carbon*, 2019, **149**, 105.

36. G. X. Han, J. B. Jia, Q. R. Liu, G. X. Huang, B. L. Xing, C. X. Zhang and Y. J. Cao, *Carbon*, 2022, **186**, 380.

37. D. Salinas Torres, R. Ruiz Rosas, M. J. Valero Romero, J. Rodríguez Mirasol, T. Cordero, E. Morallón and D. Cazorla Amorós, *J. Power Sources*, 2016, **326**, 641.